

10. DATA REPORT: GEOCHEMISTRY OF MASSIVE AND SEMIMASSIVE SULFIDES FROM SITE 1189, OCEAN DRILLING PROGRAM LEG 193¹

R.A. Binns^{2,3}

ABSTRACT

Chemical and isotopic data for rare massive and semimassive sulfide samples cored at Site 1189 (Roman Ruins, PACMANUS) suggest their genetic relationship with sulfide chimneys at the seafloor. Sand collected from the hammer drill after commencement of Hole 1189B indicates that at least the lower section of the cased interval was occupied by material similar to the stockwork zone cored from 31 to ~100 meters below seafloor (mbsf) in this hole, but with increased content of barite, sphalerite, and lead-bearing minerals. Fractional crystallization of ascending hydrothermal fluid involving early precipitation of pyrite may explain vertical mineralogical and chemical zoning within the stockwork conduit and the high base and precious metal contents of Roman Ruins chimneys. A mineralized volcanoclastic unit cored deep in Hole 1189A possibly represents the lateral fringe of the conduit system. Lead isotope ratios in the sulfides differ slightly but significantly from those of fresh lavas from Pual Ridge, implying that at least some of the Pb within the Roman Ruins hydrothermal system derived from a deeper, more radiogenic source than the enclosing altered volcanic rocks.

INTRODUCTION

Leg 193 of the Ocean Drilling Program explored the subsurface of the active PACMANUS hydrothermal field situated on Pual Ridge, a felsic

¹Binns, R.A., 2006. Data report: Geochemistry of massive and semimassive sulfides from Site 1189, Ocean Drilling Program Leg 193. *In* Barriga, F.J.A.S., Binns, R.A., Miller, D.J., and Herzig, P.M. (Eds.), *Proc. ODP, Sci. Results*, 193, 1–22 [Online]. Available from World Wide Web: <http://www-odp.tamu.edu/publications/193_SR/VOLUME/CHAPTERS/206.PDF>. [Cited YYYY-MM-DD]

²Division of Exploration and Mining, Commonwealth Scientific and Industrial Research Organisation (CSIRO), PO Box 136, North Ryde NSW 1670, Australia.

Ray.Binns@csiro.au

³Department of Earth and Marine Sciences, Australian National University, Canberra ACT 0200, Australia.

Initial receipt: 29 September 2003

Acceptance: 14 November 2005

Web publication: 4 May 2006

Ms 193SR-206

volcanic edifice rising above rifted early Tertiary arc crust in the eastern Manus backarc basin, Papua New Guinea (Binns and Scott, 1993; Binns et al., 2002; Binns, Barriga, Miller, et al., 2002). A major objective of the leg was to characterize an expected abundance of sulfide mineralization in the volcanic sequence below the seafloor and examine structural and geochemical processes that localize fields of chimneys at PACMANUS and explain their high contents of base and precious metals. However, although disseminated pyrite was found to be a widespread component in extensively altered volcanic rocks below the Snowcap (Site 1188) and Roman Ruins (Site 1189) hydrothermal sites, very few occurrences of significant sulfide mineralization were encountered, all at Site 1189. This was partly a consequence of poor core recovery, especially in an apparent stockwork zone in the upper part of Hole 1189B drilled at the crestal mound of Roman Ruins.

Although Holes 1189A and 1189B were collared 35 m apart at Roman Ruins, both beside sulfide chimneys, only three pieces of core classified as massive or semimassive sulfide (>75% and 25%–75% visually estimated abundance of sulfide minerals, respectively) were recovered (Binns, Barriga, Miller, et al., 2002). Despite the paucity of material, the aims of this study were to chemically characterize these samples and compare them with chimneys dredged from Roman Ruins (Moss and Scott, 2001; Binns et al., 2002).

SAMPLES AND METHODS

Chemical and isotopic analyses were undertaken at the Commonwealth Scientific and Industrial Research Organisation (CSIRO) (Australia) on two of these core pieces; Sample 193-1189A-12R-1 (Piece 16, 120–122 cm; CSIRO reference number 142701), representing a possible example of subhalative mineralization within a former pumiceous volcanoclastic horizon in Hole 1189A (Shipboard Scientific Party, 2002), and Sample 193-1189B-1R-1 (Piece 1, 0–4 cm; CSIRO 142703) collected from immediately below the cased interval of Hole 1189B and potentially derived from the sulfide mound presumed to underlie the Roman Ruins chimney field (Shipboard Scientific Party, 2002).

In addition, a thick semimassive pyrite vein broken from altered wallrock in Sample 193-1189B-3R-1 (Piece 4, 34–37 cm; CSIRO 142705) was chemically analyzed, whereas Pb isotope analyses were conducted on a similar vein in breccia Sample 193-1189B-5R-1 (Piece 2, 12–22 cm; CSIRO 142706). Although somewhat richer in quartz, these two subsamples were visually comparable with Sample 193-1189B-6R-1 (Piece 6, 56–67 cm) cataloged on board as massive sulfide but not sampled by the author. Like the latter, considered on this basis to be derived from an unusually thick vein rather than a horizon of massive sulfide, they represent the dominant vein style within the stockwork zone intersected in the upper part of Hole 1189B (Shipboard Scientific Party, 2002). Chemical analyses were also performed on two related samples, a 2-cm lump of massive pyrite (closely resembling Sample 193-1189B-6R-1 [Piece 6, 56–67 cm] and likely derived from the stockwork zone) caught on the bowspring of the logging tool during a geophysical survey of the uncased section of Hole 1189B (CSIRO 142808) and a sample of sand packed on the hammer drill during placement of casing at commencement of the same hole (CSIRO 142807). Details of all six samples are provided in Table T1.

For chemical analysis, representative portions (avoiding conspicuous host rock fragments or layers) were broken or sawn from the samples and the sawn surfaces were cleaned with sandpaper. After ultrasonic cleaning, washing in deionized water to remove sea salt, and drying, these were finely ground under acetone in a mechanical agate mortar and pestle. Analyses were performed by inductively coupled plasma-atomic emission spectrometry (ICP-AES) and mass spectrometry (ICP-MS) and also by instrumental neutron activation (INAA) using the CSIRO methods outlined in Miller et al. (this volume). The complete analytical data set is provided in Table T2, whereas preferred compositions taking into account precision and sensitivity of the various methods are provided in Table T3.

Lead isotope ratios (Table T4) were analyzed on separately agate-ground fragments by thermal ionization mass spectrometry on a VG54E single-collector mass spectrometer at CSIRO. Precision, based upon two relative standard deviations in 1192 analyses of the standard reference material 981, is estimated as $Pb^{206/204} = 0.16\%$, $Pb^{207/204} = 0.21\%$, and $Pb^{208/204} = 0.28\%$. Sulfur isotope ratios (Table T4) were determined for individual pyrite grains in polished slices by laser ablation mass spectrometry at the Central Science Laboratory, University of Tasmania, following the methods of Huston et al. (1995). Estimated precision of $\delta^{34}S$ relative to Canyon Diablo troilite is 0.4‰ – 0.5‰ .

RESULTS

Of the three chemically analyzed core samples (CSIRO 142701, 142703, and 142705), two have significant contents of Cu but none has other than trace levels of Zn or Pb. Contents of Ca reflect relative amounts of anhydrite-gypsum gangue, whereas other lithophile elements (Si, Al, etc.) vary in accordance with abundance of quartz gangue and wallrock particles. The massive pyrite sample collected by the logging tool contains little other than Fe and S, whereas the sand collected on the hammer drill has moderate contents of Cu and Fe; elevated Zn, Pb, Ca, and Ba; and lithophile elements attributable to altered country rock particles. In terms of the dominant chalcophile elements, all five samples are distinctly poorer in Cu and Zn than sulfide chimneys from Roman Ruins (Fig. F1).

Table T5 lists normative mineralogical constitutions computed as follows. First, sulfur was allocated with Ca, Ba, Pb, and Zn to form anhydrite, barite, galena, and Fe-free sphalerite, respectively, then S with Cu and Fe to form chalcopyrite, and, finally, remaining S with remaining Fe to form pyrite or, where Fe is deficient, to pyrite and pyrrhotite. Normative silicate content (including any residual Fe) is calculated as the difference from 100% total, and thereby includes H_2O , which was not determined. The results agree well with the observed mineralogy of the samples (Table T1) except for pyrrhotite, which is unrecorded microscopically but whose minor normative presence is explicable by levels of analytical precision.

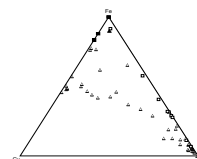
Table T6 provides estimated compositions for the silicate gangue components of the samples, calculated after subtracting normative sulfides and sulfates and reconstituting the residue to total 100%. The indicated FeO and CaO contents are highly subject to analytical error and to assumptions made when calculating normative sulfides and sulfates and take no account of the disseminated pyrite present in wallrock fragments. As observed by optical microscope, quartz gangue is almost ex-

T2. Sulfide data set, p. 15.

T3. Sulfide and Roman Ruin chimneys compositions, p. 18.

T4. Isotope data, p. 20.

F1. Sulfide composition, p. 10.



T5. Normative compositions, p. 21.

T6. Silicate bulk compositions, p. 22.

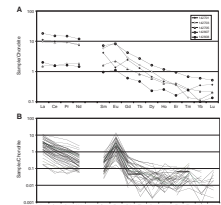
clusive in semimassive pyrite sample CSIRO 142705 and predominant (with some aluminous wallrock) in mineralized volcanoclastic sample CSIRO 142701. In the sand from the hammer drill (CSIRO 142807), the bulk silicate composition (arising from wallrock fragments) is broadly comparable with that of an illite-dominated wallrock sample collected just below the casing in Hole 1189B (Sample 193-1189B-1R-1 [Piece 2, 10–14 cm]) (Shipboard Scientific Party, 2002, and new data), but for semimassive sulfide CSIRO142703, also from just below the casing, the indicated nature of wallrock contaminants is more chloritic. The computed composition for scarce wallrock particles in the logging tool sample of massive pyrite (CSIRO 142808) is uncommonly rich in Fe and Mn. The Fe value is probably a spurious outcome of the calculation compounded by low abundance of the silicate component (<5%), but Mn is unexplained.

Relative to the average composition of Roman Ruins chimneys (Table T3), Leg 193 massive and semimassive sulfides are enriched in Co, Te, and Bi and mildly enriched in Se. These chalcophile trace elements, apart from Bi, concentrate within pyrite in PACMANUS chimneys (Binns et al., 2002); therefore, their enrichment reflects subsurface abundance of this mineral. However, contents of Mo and Tl, also concentrated in chimney pyrite, are similar. The habitat of enriched Bi, normally concentrated in chalcopyrite, is unknown for the Leg 193 samples. The latter are depleted relative to chimneys in Ga, Ge, and Cd (which concentrate in chimney sphalerite), in In (concentrated in chimney chalcopyrite and tennantite), and in As, Ag, and Sb (concentrated in chimney sulfosalts, particularly dufrenoyite). Au is a significant trace element in the three leg samples analyzed by INAA. Its abundance is less than the chimney average but falls within the lower range of the chimney population. Native Au has not been identified microscopically in any sample examined in this study. Contents of Sr correlate with anhydrite abundance, whereas those of other lithophile trace elements relate to abundance of wallrock fragments, though with some anomalies, such as the high U in CSIRO 142807, the sand recovered from the hammer drill from within the cased interval of Hole 1189B.

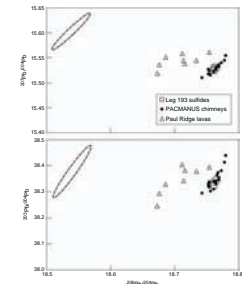
Rare earth element (REE) abundances in Leg 193 massive and semimassive sulfides span the higher range of Roman Ruins chimneys (Fig. F2). Chondrite-normalized profiles of the latter (Fig. F2B), where REEs are contained principally in barite or rarer anhydrite, show pronounced light REE (LREE) enrichment ($La_N/Yb_N = \sim 70$) and distinct positive Eu anomalies ($Eu/Eu^* = \sim 15$). Leg 193 samples show similar LREE enrichment patterns but subdued Eu anomalies ranging from slightly positive to negative (Fig. F2A). The variability in Eu/Eu^* arises from the combined presence of anhydrite, which displays variable but mostly positive Eu enrichment, and altered wallrock fragments that tend to show significant Eu depletion (Bach et al., 2003).

Lead isotope ratios of the three Leg 193 samples analyzed are identical within precision limits to those of Roman Ruins chimneys, but like the latter they differ slightly yet significantly from those of fresh volcanic glasses at Pual Ridge, ranging from andesite to rhyodacite in composition (Fig. F3). Sulfur isotope ratios of Leg 193 pyrites also span the range of values measured in Roman Ruins chimneys (Fig. F4). These results are consistent with a cogenetic relationship between the seafloor and subsurface mineralization, with the important implication that the source of Pb in both was more radiogenic overall than the lavas constituting Pual Ridge. Whereas some of the Pb in chimneys and the subsur-

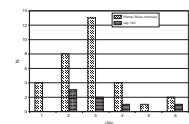
F2. Rare earth element patterns, p. 11.



F3. Lead isotope ratios, p. 12.



F4. Sulfur isotope measurements, p. 13.



face massive and semimassive sulfides was potentially leached from the volcanic sequence during alteration, some must also derive from another source, most likely by leaching of basement rocks underlying the volcano in the deeper reaction zone of the PACMANUS hydrothermal system. The sulfur isotope data are consistent with the interpretation that a proportion of S^{2-} in the PACMANUS hydrothermal fluids was of igneous provenance ($\delta^{34}S = \sim 0\text{‰}$) mixed with a variable component derived by reduction of seawater sulfate ($\delta^{34}S = \sim +4$ to $+6\text{‰}$ for equilibrium reduction at 350° – $400^{\circ}C$; Shanks, 2001, fig. 9). Since fresh Pual Ridge lavas contain negligible S (<100 ppm), a deeper magmatic source is suggested for the igneous component rather than leaching from Pual Ridge lavas during their alteration within the PACMANUS hydrothermal system. Sr and S isotope studies of Leg 193 anhydrites also suggest mixing between seawater and an igneous component (Roberts et al., 2003).

DISCUSSION

The sand collected by the hammer drill (CSIRO 142807) provides our only tangible indication of what occurred in the topmost cased interval of Hole 1189B, though it is not known whether it represents the entire interval or only its lower section. During the hammer-in casing operation, penetration was fast (7 m/hr) from seabed to 7 meters below seafloor (mbsf), and then slow (1 m/hr) between 7 and 8 mbsf. It sped up from 8 to 10 mbsf, but slowed to <1 m/hr between 10 and 15 mbsf before suddenly increasing remarkably to >30 m/hr until the casing operation ended at 30 mbsf (Shipboard Scientific Party, 2002). Although it seems reasonable to infer that the hard layers were unaltered dacite, no such material is present in the sand. Rather, the sand contains three main kinds of particle: (1) soft altered dacite fragments, (2) compact sulfide aggregates dominated by coarse pyrite euhedra that more closely resemble massive sulfide veins from the stockwork zone than the seafloor chimneys (where pyrite is scarce and more commonly fine grained and botryoidal), and (3) aggregates of coarse anhydrite. This suggests that whatever part of the cased interval the sample represents was basically similar to the underlying stockwork zone cored from 31 to ~ 100 mbsf in Hole 1189B. However, the bulk geochemistry of the sand indicates that sphalerite and barite, as well as Pb and Au, are significantly more abundant somewhere in the cased interval than in the semimassive sulfide core sample from immediately below the casing.

From an expedition undertaken after Leg 193 at Roman Ruins, in the vicinity of Hole 1189B, Petersen et al. (2003) report a variety of massive sulfide types in shallow diamond cores drilled as far as 5 mbsf, all highly enriched in base and precious metals. These include chimney fragments and apparently resedimented sulfide material plus nodular breccias with chalcopyrite-pyrite clasts set in an anhydrite matrix. The latter are remarkably similar to and likely cogenetic with the semimassive sulfide sample (CSIRO 142703) from immediately below the casing of Hole 1189B. Some holes bottomed in weakly to intensely clay-altered dacite, locally with stockworklike sulfide veining. Although a "missing link" remains, these results and the data for sample CSIRO 142807 collectively suggest that in Hole 1189B the sulfide-veined stockwork zone with fragments of altered dacite persists almost to the seafloor, perhaps with some thin intervals of harder, fresh, or less altered dacite and pods of semimassive sulfide resembling sample CSIRO 142703, and possibly

with an upward-increasing abundance of sphalerite and barite. Rapid lateral change is indicated, however, by the cores of Hole 1189A drilled only ~35 m west-southwest from Hole 1189B adjacent to a chimney ~8 m lower on the Roman Ruins mound. Here, a thin interval of fresh dacite (represented by only 17 cm of recovered core) occurred directly below the 3-m jet-in test interval and passed gradationally downward into altered dacite lacking the sulfide stockwork (Shipboard Scientific Party, 2002). Geophysical logging of uncored Hole 1189C, drilled ~31 m east-southeast of Hole 1189B and 7 m lower on the opposite side of the mound crest from Hole 1189A, indicates only limited sulfide occurrence relative to the stockwork zone of Hole 1189B (Bartetzko et al., 2003). Taken together, results of the deep and shallow drilling establish that the stockwork zone in the upper part of Hole 1189B and related but unidentified subsidiary fractures represent the conduit for upward passage of high-temperature hydrothermal fluid responsible for growth of sulfide chimneys at Roman Ruins. However, the main conduit is clearly limited in lateral extent, at least in the direction of a section linking Holes 1188A, 1188B, and 1188C.

If account is taken of the predominance of pyrite in the Site 1189 subsurface massive and semimassive sulfides, their elemental constitution relative to Roman Ruins chimneys is consistent with a genetic relationship between the two groups. This is further indicated by isotopic data presented above, lending support to the interpretation (Shipboard Scientific Party, 2002) that the pyritic stockwork zone intersected in the higher part of Hole 1189B represents the subsurface plumbing system for hydrothermal fluids venting at the seafloor and forming the Roman Ruins chimneys. The mineralized pumice breccia of Hole 1189A (CSIRO 142701) occurs outside this stockwork, but its mineralogy, chemistry, and Pb and S isotopic composition suggest it also belongs to the conduit system, perhaps formed at its fringe by subhalative sulfide deposition in a formerly permeable volcanoclastic horizon.

Given exceptionally poor core recovery in the stockwork zone, the samples are too few for a thorough assessment of these relationships. Some samples from the stockwork zone possess thin quartz veins of uncertain temporal relationship to the more common massive to semimassive pyrite veins and breccia matrixes. One such vein in Sample 193-1189B-8R-1 (Piece 15, 68–70 cm; CSIRO 142710) contains significant chalcopyrite, in excess of pyrite, and disseminated chalcopyrite is also common in its adjacent selvage of silicified wallrock. In the lower sequence of Hole 1189B intersected below the stockwork zone, Sample 193-1189B-13R-1 (Piece 7, 35–38 cm; CSIRO 142717) contains a thin quartz vein with pyrite, sphalerite, lesser chalcopyrite, and significant barite. [Pinto et al.](#) (this volume) report additional examples of thin veins with chalcopyrite and sphalerite from the lower sequence, including one with native gold and one with galena. Mineralogically, these have a closer prima facie affinity with the Roman Ruins chimneys than the dominant massive to semimassive pyrite veins of the stockwork zone. Possibly, however, they represent an earlier phase in the hydrothermal history, or alternatively they were deposited in the fringes of the main Roman Ruins hydrothermal system. If the massive and semimassive sulfide veins of the stockwork indeed constitute the main subsurface conduits for the Roman Ruins system, then the results and discussion presented here suggest a pronounced vertical zoning arising from fractional crystallization, whereby pyrite precipitates at depth and the ascending fluid becomes progressively enriched in Cu, Zn, and Pb. Chalcopyrite then sphalerite commence precipitation at levels just be-

low and within the cased interval of Hole 1189B, whereas Pb remains primarily in solution until formation of galena and sulfosalts immediately below the seafloor (lower mound) and in the chimneys. This is a similar order of mineral precipitation to that modeled by Bowers et al. (1985) for East Pacific Rise hydrothermal fluids during either conductive cooling or mixing with cold seawater. Subsurface phase separation as indicated by fluid inclusions in Leg 193 anhydrites (Vanko et al., 2004) will complicate this simplistic model which, nevertheless, offers an alternative explanation to "zone refining" for the uncommonly high contents of base and precious metals in Roman Ruins and other PAC-MANUS chimneys. A similar contrast between chemistry of chimneys and that of a subsurface stockwork zone was established by Ocean Drilling Program Leg 158 at the basalt-hosted Trans-Atlantic Geotraverse hydrothermal site (Herzig et al., 1998; Petersen et al., 2000).

ACKNOWLEDGMENTS

Lesley Dotter and Barbara Gardner of CSIRO are thanked for chemical and Pb isotope analyses, respectively, and Robina Sharpe and Keith Harris (University of Tasmania) for S isotope microanalyses. This research used samples provided by the Ocean Drilling Program (ODP). ODP is sponsored by the U.S. National Science Foundation (NSF) and participating countries under management of Joint Oceanographic Institutions (JOI), Inc. Funding was provided by CSIRO and the P2+ consortium of Australian mineral companies.

REFERENCES

- Bach, W., Roberts, S., Vanko, D.A., Binns, R.A., Yeats, C.J., Craddock, P.R., and Humphris, S.E., 2003. Controls of fluid chemistry and complexation on rare earth element contents of anhydrite from the PACMANUS seafloor hydrothermal system, Manus Basin, Papua New Guinea. *Miner. Deposita*, 38(8):916–935.
- Bartetzko, A., Paulick, H., Iturrino, G., and Arnold, J., 2003. Facies reconstruction of a hydrothermally altered dacite extrusive sequence—evidence from geophysical downhole logging data (ODP Leg 193). *Geochem., Geophys., Geosyst.*, 4:1087. [doi:10.1029/2003GC000575](https://doi.org/10.1029/2003GC000575)
- Binns, R.A., Barriga, F.J.A.S., Miller, D.J., et al., 2002. *Proc. ODP, Init. Repts.*, 193 [CD-ROM]. Available from: Ocean Drilling Program, Texas A&M University, College Station TX 77845-9547, USA. [\[HTML\]](#)
- Binns, R.A., McConachy, T.F., Parr, J.M., and Yeats, C.J., 2002. The PACMANUS Memoir (P2+). *CSIRO Exploration and Mining Report 1032C* [CD-ROM]. Available from: CSIRO Exploration and Mining, North Ryde NSW 1670, Australia.
- Binns, R.A., and Scott, S.D., 1993. Actively forming polymetallic sulfide deposits associated with felsic volcanic rocks in the eastern Manus back-arc basin, Papua New Guinea. *Econ. Geol.*, 88:2226–2236
- Bowers, T.S., Von Damm, K.L., and Edmond, J.M., 1985. Chemical evolution of mid-ocean ridge hot springs. *Geochim. Cosmochim. Acta*, 49:2239–2252. [doi:10.1016/0016-7037\(85\)90224-8](https://doi.org/10.1016/0016-7037(85)90224-8)
- Herzig, P.M., Petersen, S., and Hannington, M.D., 1998. Geochemistry and sulfur-isotopic composition of the TAG hydrothermal mound, Mid-Atlantic Ridge, 26°N. In Herzig, P.M., Humphris, S.E., Miller, D.J., and Zierenberg, R.A. (Eds.), *Proc. ODP, Sci. Results*, 158: College Station, TX (Ocean Drilling Program), 47–70. [\[PDF\]](#)
- Huston, D.L., Power, M., Gemmell, J.B., and Large, R.R., 1995. Design, calibration and geological application of the first operational Australian laser ablation sulphur isotope microprobe. *Aust. J. Earth Sci.*, 42:549–555.
- Moss, R., and Scott, S.D., 2001. Geochemistry and mineralogy of gold-rich hydrothermal precipitates from eastern Manus Basin, Papua New Guinea. *Can. Mineral.*, 39:957–978.
- Parr, J.M., Binns, R.A., Yeats, C.J., Carr, G.C., and Gardner, B.L., 2000. Lead isotope characteristics of volcanic rocks and hydrothermal sulfide deposits from the Eastern Manus Basin and Franklin Seamount, Papua New Guinea: evidence for the Pacific-Indian mantle boundary. *Geol. Soc. Aust., Abstr.*, 59:378.
- Petersen, S., Herzig, P.M., and Hannington, M.D., 2000. Third dimension of a presently forming VMS deposit: TAG hydrothermal mound, Mid-Atlantic Ridge, 26°N. *Miner. Deposita*, 35:233–259.
- Petersen, S., Herzig, P.M., Hannington, M.D., and Gemmell, J.B., 2003. Gold-rich massive sulfides from the interior of the felsic-hosted PACMANUS massive sulfide deposit, Eastern Manus Basin (PNG). In Eliopoulos, D.G. et al. (Eds.), *Mineral Exploration and Sustainable Development*: Rotterdam (Millpress), 171–174.
- Roberts, S., Bach, W., Binns, R.A., Vanko, D.A., Yeats, C.J., Teagle, D.A.H., Blacklock, K., Blusztajn, J.S., Boyce, A.J., Cooper, M.J., Holland, N., and McDonald, B., 2003. Contrasting evolution of hydrothermal fluids in the PACMANUS system, Manus Basin; the Sr and S isotope evidence. *Geology*, 31:805–808. [doi:10.1130/G19716.1](https://doi.org/10.1130/G19716.1)
- Shanks, W.C., III, 2001. Stable isotopes in seafloor hydrothermal systems: vent fluids, hydrothermal deposits, hydrothermal alteration, and microbial processes. In Valley, J.W., and Cole, D.R. (Eds.), *Stable Isotope Geochemistry*. *Rev. Mineral. Geochem.*, 43:469–525. [doi:10.1130/G19716.1](https://doi.org/10.1130/G19716.1)
- Shipboard Scientific Party, 2002. Site 1189. In Binns, R.A., Barriga, F.J.A.S., Miller, D.J., et al., *Proc. ODP, Init. Repts.*, 193 [CD-ROM]. Available from: Ocean Drilling Program, Texas A&M University, College Station TX 77845-9547, USA. [\[HTML\]](#)

Vanko, D.A., Bach, W., Roberts, S., Yeats, C.J., and Scott, S.D., 2004. Fluid inclusion evidence for subsurface phase separation and variable fluid mixing regimes beneath the deep-sea PACMANUS hydrothermal field, Manus Basin back-arc rift, Papua New Guinea. *J. Geophys. Res.*, 109:B03201. doi:[10.1029/2003JB002579](https://doi.org/10.1029/2003JB002579)

Figure F1. Ternary composition plot (in weight percent) for Leg 193 semimassive sulfides (black squares; two samples at the Fe apex) compared with subsamples from Roman Ruins chimneys (open triangles). Open squares are subsamples from the “Bikpela” chimney, also from Roman Ruins. The black triangle is a sand collected by hammer drill from the cased interval of Hole 1189B. Chimney data are from Binns et al. (2002), with some additional analyses.

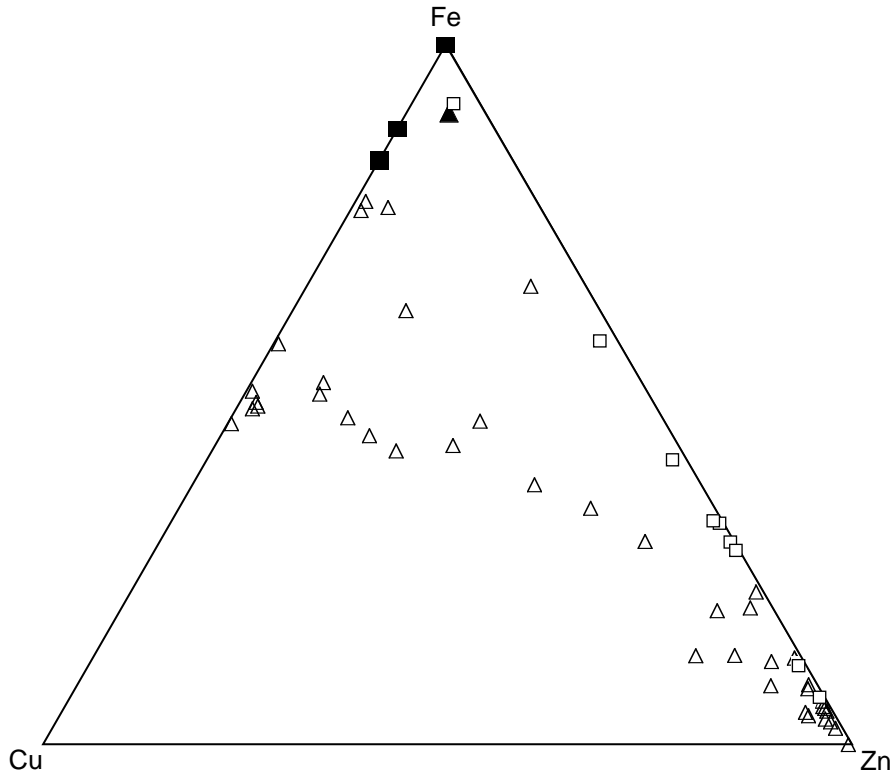


Figure F2. Chondrite-normalized rare earth element patterns (ICP-MS) of (A) Leg 193 semimassive sulfides compared to (B) Roman Ruins chimneys. Data for HREE >Gd are close to the detection limit, and only the general trend is significant. Data from Binns et al. (2002) and additional data.

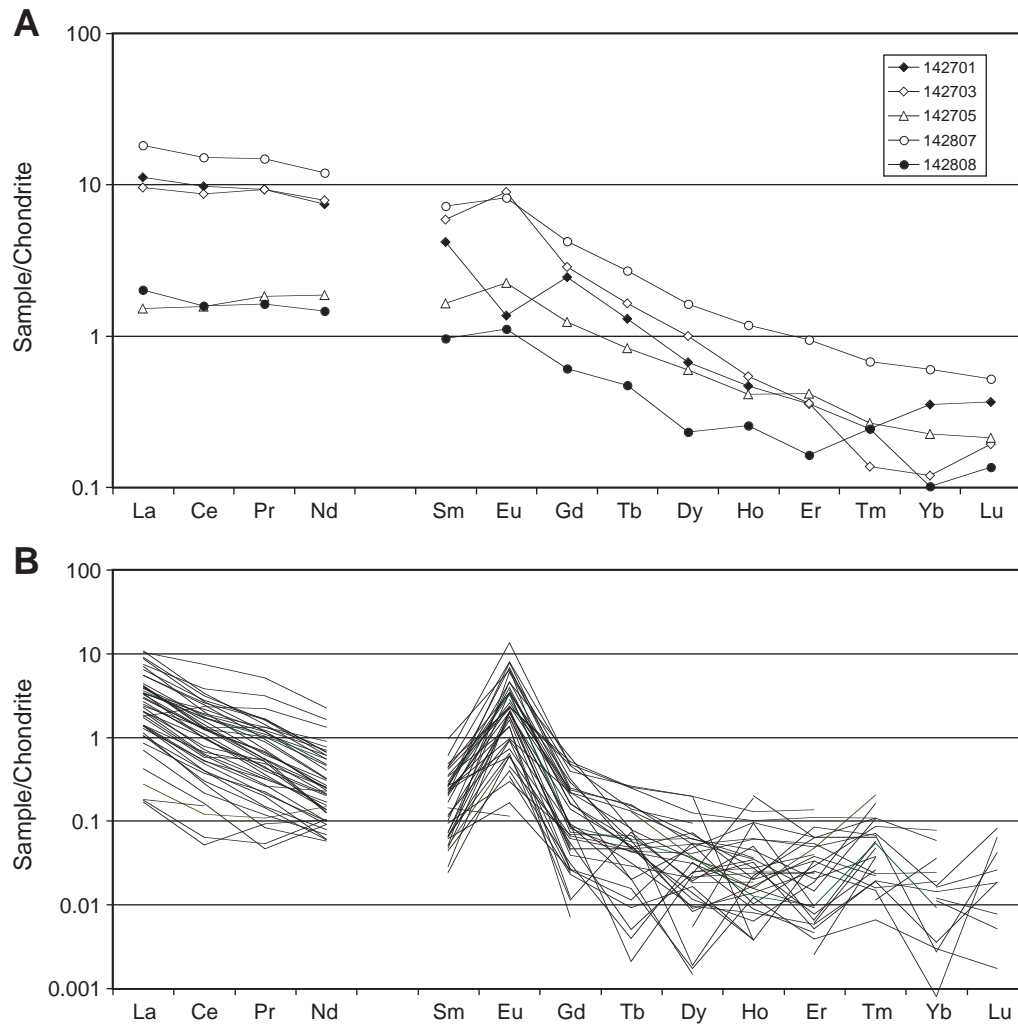


Figure F3. Lead isotope ratio plots showing similarity of Leg 193 sulfides (Site 1189) to PACMANUS chimneys (Parr et al., 2000; Binns et al., 2002), both being statistically more radiogenic than glassy lavas from Pual Ridge. Dashed ellipses indicate analytical precision.

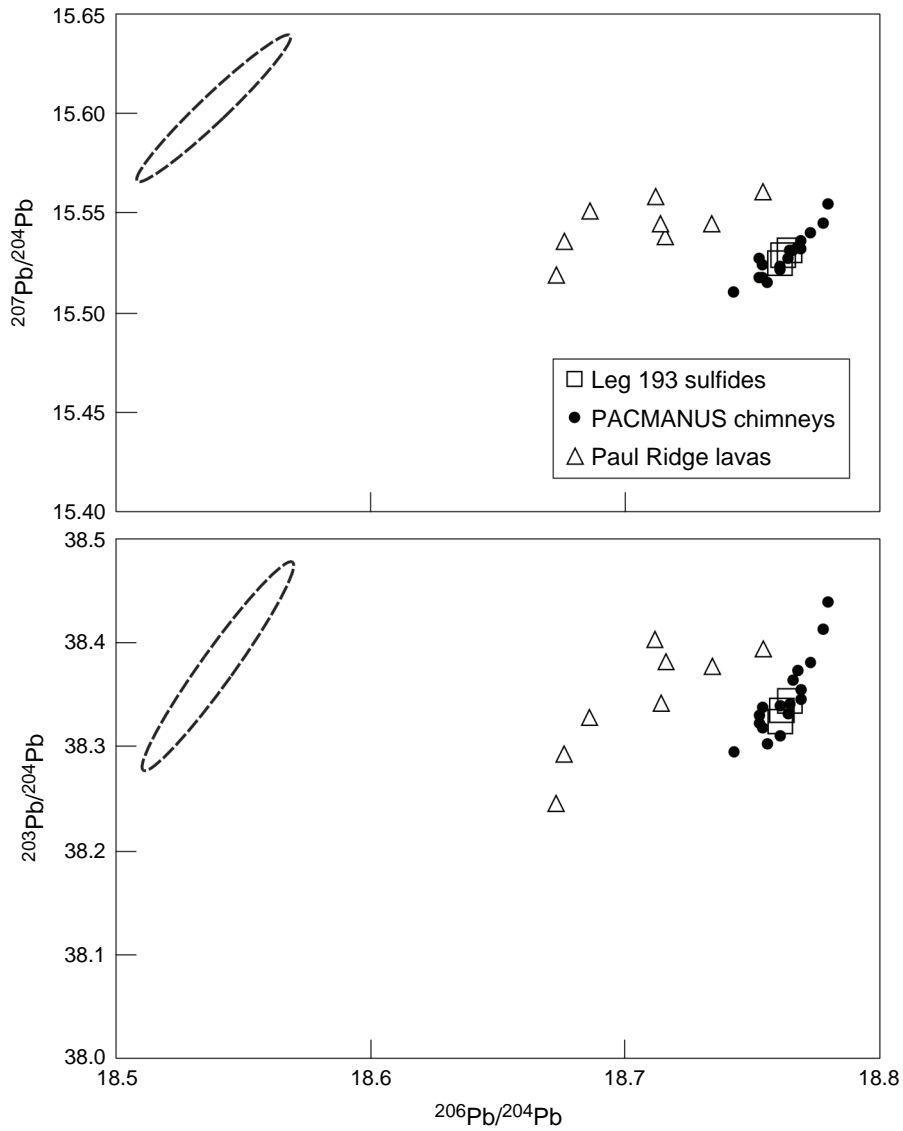


Figure F4. Histogram of sulfur isotope measurements on pyrite from Leg 193 semimassive sulfides compared to sulfides (pyrite, chalcopyrite, and sphalerite) in chimneys from Roman Ruins (Binns et al., 2002).

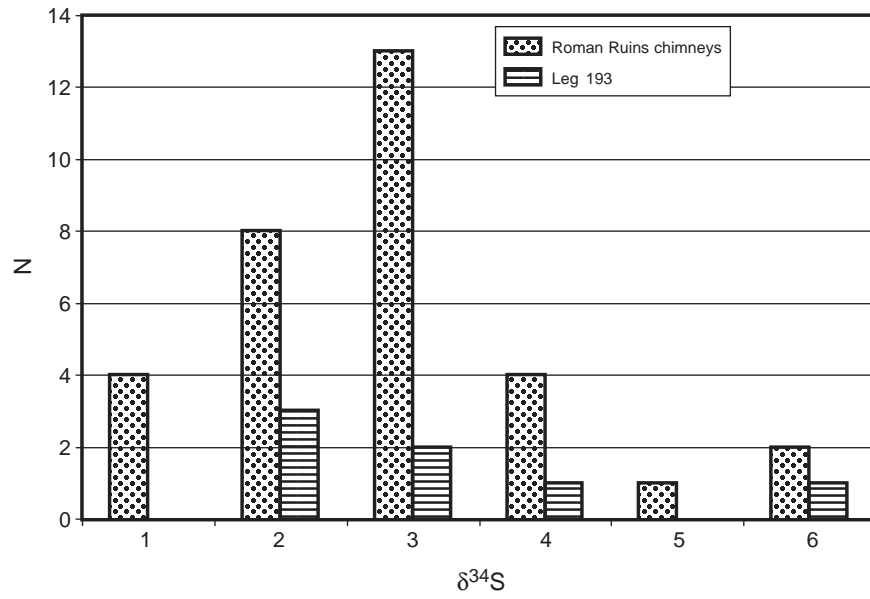


Table T1. Massive and semimassive sulfide sample details.

Core, section, interval (cm)	CSIRO number	Curated depth (mbsf)	Description
193-1189A-12R-1 (Piece 16, 120–122)	142701	107.70	Mineralized volcanoclastic with altered tube pumice and nonvesicular fragments. Slice cut from the semimassive sulfide interval, where wallrock clasts are dispersed and matrix-supported by granular quartz-pyrite vein material with minor replacement veinlets along fractures. Chalcopyrite is concentrated in vague layers, intergrown with pyrite and quartz and locally mantling the former. Traces of anhydrite intergrown with matrix quartz, and rare sphalerite and magnetite inclusions in pyrite.
193-1189B-1R-1 (Piece 1A, 0–4)	142703	31.00	Semimassive sulfide with irregular aggregates or nodules of intergrown pyrite-chalcopyrite set within a bladed to granular anhydrite-gypsum-pyrite-(chalcopyrite) matrix. Local patches of anhydrite-gypsum with scarce sulfides. Euhedral pyrites border many aggregates. Chalcopyrite forms ragged overgrowths on pyrite and also inclusions within pyrite. Rare sphalerite as inclusions in pyrite. Small fragments of altered, vaguely perlitic wallrock with finer grained disseminated pyrite are scattered through the rock.
3R-1 (Piece 4, 34–37)	142705	50.04	Semimassive sulfide composed of granular quartz and pyrite, free of anhydrite, with some euhedral quartz terminations developed in drusy cavities. Sample as provided was evidently broken from a thick vein in altered wallrock. Slice sawn to avoid wallrock fragments along one side.
5R-1 (Piece 2, 12–22)	142706	69.42	Jigsaw-fit breccia with white, altered perlitic wallrock fragments just supported by a matrix (locally veinlike) of coarse-grained, semimassive pyrite and quartz. The pyrite tends to form clusters with euhedral faces at their border. Quartz mostly granular but shows euhedral terminations in drusy cavities, overgrown by rare anhydrite blades. Sample was broken, and matrix fragments hand-picked for Pb isotope analysis.
Sand packed on hammer drill.	142807	<31	Contains particles to 5 mm diameter. Subequal proportions of massive sulfide and pale creamy altered wallrock fragments (with fine-grained disseminated pyrite), and rarer aggregates of bladed white anhydrite (scarce gypsum), some with pyrite inclusions. The massive sulfide particles are compact and predominantly composed of euhedral and subhedral pyrite grains up to 0.2 mm across. Occasional black particles with sphalerite and scarce barite blades. No quartz grains or particles of unaltered dacite. Portion of sample finely ground for analysis.
Lump caught on bowspring of logging tool.	142808	>35 (<100?)	Massive pyrite with numerous small cavities lined by euhedral crystals. Neither quartz nor anhydrite is present, but there are a few small fragments of creamy white altered dacite with disseminated pyrite. Resembles many veins from the stockwork zone in Hole 1189B (31 m to ~100 mbsf), lacking in the lower sequence >120 mbsf. Portion of sample sawn off for analysis.

Note: CSIRO = Commonwealth Scientific and Industrial Research Organisation.

Table T2. Complete analytical data set for massive and semimassive sulfides. (See table notes. Continued on next two pages.)

CSIRO number	Element:	Li	Be	Na	Na	Mg	Al	Si	P	S	K	K	Ca	Ca
	Method:	ICP-AES	ICP-AES	ICP-AES	INAA	ICP-AES	ICP-AES	ICP-AES*	ICP-AES	ICP-AES	ICP-AES	INAA	ICP-AES	INAA
	Unit: DL:	(ppm) 5	(ppm) 2	(ppm)	(wt%) 0.01	(ppm)	(ppm)	(ppm)	(ppm) 50	(ppm)	(ppm)	(wt%) 0.2	(ppm)	(wt%) 0.5
142701		2.2	0.2	1,305		1,850	12,946	170,907	9	274,664	5,966		3,951	
142703		0.8	0.1	227	0.04	2,794	1,680	5,690	ND	361,547	ND	<0.2	91,275	9.8
142705		2.6	0.2	67		78	1,716	272,319	359	202,880	342		856	
142807		16.9	0.2	2,295	0.25	2,954	22,012	40,356	187	366,125	9,149	0.9	15,533	1.9
142808		0.1	0.1	315	0.05	608	1,186	6,326	ND	509,130	481	<0.2	188	<0.5

CSIRO number	Element:	Sc	Sc	Sc	Ti	V	V	Cr	Cr	Cr	Mn	Fe	Fe	Co
	Method:	ICP-AES	ICP-MS	INAA	ICP-AES	ICP-AES	ICP-MS	ICP-AES	ICP-MS	INAA	ICP-AES	ICP-AES	INAA	ICP-AES
	Unit: DL:	(ppm) 5	(ppb) 100	(ppm) 0.1	(ppm)	(ppm) 5	(ppb)	(ppm) 5	(ppb)	(ppm) 10	(ppm)	(ppm)	(wt%)	(ppm)
142701		2.3	2,390		905	30	28,423	2	4,400		43	234,331		620
142703		ND	156	0.4	48	2	2,374	ND	1,053	<10	73	254,353	27	73
142705		ND	81		24	2	4,530	2	6,927		101	188,821		60
142807		2.3	3,312	4.6	1,189	23	20,500	46	47,360	57	282	300,729	32	93
142808		ND	545	0.4	56	1	1,315	ND	1,181	<10	209	439,006	47	95

CSIRO number	Element:	Co	Co	Ni	Ni	Cu	Zn	Zn	Ga	Ge	As	As	As	Se
	Method:	ICP-MS	INAA	ICP-AES	ICP-MS	ICP-AES	ICP-AES	INAA	ICP-MS	ICP-MS	ICP-AES	ICP-MS	INAA	INAA
	Unit: DL:	(ppb)	(ppm)	(ppm) 10	(ppb)	(ppm)	(ppm)	(ppm) 100	(ppb)	(ppb)	(ppm)	(ppb)	(ppm)	(ppm)
142701		OR		12	10,570	32,267	232		11,516	6,191	89	79,758		
142703		66,140	80	ND	2,854	50,423	638	640	1,100	5,481	231	217,900	741	42
142705		56,083		10	7,651	114	276		405	3,721	271	OR		
142807		81,655	95	34	30,055	15,801	16,394	18,100	12,855	10,525	269	256,550	1,020	47
142808		80,830	98	ND	1,253	1,142	451	507	649	8,060	204	191,000	629	78

Table T2 (continued).

CSIRO number	Element:	Br	Rb	Rb	Sr	Y	Y	Zr	Zr	Mo	Mo	Mo	Ag	Ag
	Method:	INAA	ICP-MS	INAA	ICP-AES	ICP-AES	ICP-MS	ICP-AES	INAA	ICP-AES	ICP-MS	INAA	ICP-AES	INAA
	Unit: DL:	(ppm) 1	(ppb)	(ppm) 20	(ppm)	(ppm) 2	(ppb)	(ppm) 5	(ppm) 500	(ppm)	(ppb)	(ppm)	(ppm) 5	(ppm) 5
142701			8,252		10	3.4	961	15		65	64,042		1.3	
142703	1	265	21	574	0.8	943	9	<500	70	75,580	69	2.5	<5	
142705		647		13	1.1	778	4		76	76,029		0.7		
142807	12	14,985	44	199	2.2	2,298	17	<500	68	74,125	65	14.8	13.2	
142808	3	1,059	22	5	0.3	428	8	<500	41	45,730	42	1.3	<5	

CSIRO number	Element:	Cd	Cd	Cd	In	Sb	Sb	Sb	Te	Te	Cs	Cs	Ba	Ba
	Method:	ICP-AES	ICP-MS	INAA	ICP-MS	ICP-AES	ICP-MS	INAA	ICP-MS	INAA	ICP-MS	INAA	ICP-AES	INAA
	Unit: DL:	(ppm) 5	(ppb)	(ppm) 20	(ppb)	(ppm) 50	(ppb)	(ppm) 0.2	(ppb) 90	(ppm) 10	(ppb) 10	(ppm) 2	(ppm)	(ppm) 100
142701		5	576		771	8	2,732		71,728		71		286	
142703		7	1,826	<20	2,802	14	5,506	4.9	168	<10	9	<2	78	118
142705		ND	1,187		276	13	3,522		5,566		60		100	
142807		64	56,825	81	4,244	59	47,170	48.1	4,856	<10	187	<2	101	10,400
142808		6	887	<20	436	21	2,041	1.4	3,613	<10	64	<2	145	206

CSIRO number	Element:	La	La	La	Ce	Ce	Pr	Nd	Sm	Sm	Eu	Eu	Gd	Tb
	Method:	ICP-AES	ICP-MS	INAA	ICP-MS	INAA	ICP-MS	ICP-MS	ICP-MS	INAA	ICP-MS	INAA	ICP-MS	ICP-MS
	Unit: DL:	(ppm)	(ppb)	(ppm) 0.5	(ppb)	(ppm) 2	(ppb)	(ppb)	(ppb)	(ppm)	(ppb)	(ppm) 0.5	(ppb)	(ppb)
142701		4.1	4,083		9,280		1,275	5,278	966		118		749	75
142703		3.7	3,512	3.6	8,325	9	1,273	5,568	1,359	1.4	778	0.8	875	95
142705		0.7	556		1,486		250	1,319	377		194		376	48
142807		6.9	6,680	8.2	14,515	17	2,030	8,481	1,665	2.1	712	0.8	1,288	155
142808		0.5	738	0.9	1,504	2	223	1,036	222	0.4	97	<0.5	185	27

Table T2 (continued).

CSIRO number	Element:	Dy	Ho	Er	Tm	Yb	Yb	Yb	Lu	Lu	Hf	Ta	W	Ir
	Method:	ICP-MS	ICP-MS	ICP-MS	ICP-MS	ICP-AES	ICP-MS	INAA	ICP-MS	INAA	INAA	INAA	INAA	INAA
	Unit: DL:	(ppb)	(ppb)	(ppb)	(ppb)	(ppm)	(ppb)	(ppm)	(ppb)	(ppm)	(ppm)	(ppm)	(ppm)	(ppb)
						2		0.5		0.2	1	1	2	20
142701		254	40	88	9	0.3	87		14					
142703		379	46	89	5	ND	30	<0.5	7	<0.2	<1	<1	<2	<20
142705		226	35	104	9	ND	56		8					
142807		620	100	235	24	ND	148	0.9	20	<0.2	1.1	<1	11	<20
142808		88	22	41	9	ND	25	<0.5	5	<0.2	<1	<1	<2	<20

CSIRO number	Element:	Au	Hg	Tl	Pb	Pb	Bi	Th	Th	U	U
	Method:	INAA	INAA	ICP-MS	ICP-AES	ICP-MS	ICP-MS	ICP-MS	INAA	ICP-MS	INAA
	Unit: DL:	(ppb)	(ppm)	(ppb)	(ppm)	(ppb)	(ppb)	(ppb)	(ppm)	(ppb)	(ppm)
		5	5					5	0.5		2
142701				5,020	112	77,947	36,211	392		687	
142703		858	5	33,160	104	78,220	15,450	8	<0.5	441	<2
142705				116,356	187	158,020	33,788	11		155	
142807		1,970	6	41,000	491	OR	14,470	159	<0.5	2,460	2.7
142808		1,990	9	27,250	115	109,200	17,610	31	<0.5	783	<2

Notes: CSIRO = Commonwealth Scientific and Industrial Research Organisation, ICP-AES = inductively coupled plasma-atomic emission spectroscopy, ICP-MS = inductively coupled plasma-mass spectrometry, INAA = instrumental neutron activation analysis. DL = detection limit (cited where close to or exceeding some values). ND = not detected, OR = over range. Sample 142807 had a white residue present on dissolution; S, Ba, and Pb may be underestimated in ICP data, * = closed-vessel dissolution. As by ICP-AES and ICP-MS may be underestimated at this level if As not fully oxidized during dissolution. Zr data by ICP-AES may be unreliable at this level. See Table T1, p. 14, for ODP sample identifications for CSIRO numbers.

Table T3. Preferred compositions of Leg 193 massive and semimassive sulfides and average Roman Ruins chimneys. (See table notes. Continued on next page.)

CSIRO number	Element:	Li	Be	Na	Mg	Al	Si	P	S	K	Ca	Sc	Ti
	Method:	ICP-AES	ICP-AES	ICP-AES	ICP-AES	ICP-AES	ICP-AES	ICP-AES	ICP-AES	ICP-AES	ICP-AES	ICP-MS	ICP-AES
	Unit: DL:	(ppm) 5	(ppm) 2	(ppm)	(ppm)	(wt%)	(wt%)	(ppm) 50	(wt%)	(ppm) 50	(ppm)	(ppm) 0.1	(ppm)
142701		<5	<2	1,305	1,850	1.29	17.09	9	27.5	5,966	3,951	2.4	905
142703		<5	<2	227	2,794	0.17	0.57	<50	36.2	<50	9.13%	0.16	48
142705		<5	<2	67	78	0.17	27.23	359	20.3	342	856	0.08	24
142807		17	<2	2,295	2,954	2.20	4.04	187	36.6	9,149	1.55%	3.3	1,189
142808		<5	<2	315	608	0.12	0.63	<50	50.9	481	188	0.55	56
Roman Ruins chimneys		<5	<2	960	190	720 (ppm)	2.1	29	25	160	210	1.1	4

CSIRO number	Element:	V	Cr	Mn	Fe	Co	Ni	Cu	Zn	Ga	Ge	As	Se
	Method:	ICP-MS	ICP-MS	ICP-AES	ICP-AES	ICP-MS	ICP-MS	ICP-AES	ICP-AES	ICP-MS	ICP-MS	INAA	INAA
	Unit: DL:	(ppm)	(ppm)	(ppm)	(wt%)	(ppm)	(ppm)	(wt%)	(ppm)	(ppm)	(ppm)	(ppm)	(ppm)
142701		28.4	4.4	43	23.4	620*	10.6	3.23	232	11.5	6.2	89**	
142703		2.4	1.1	73	25.4	66	2.9	5.04	638	1.1	5.5	741	42
142705		4.5	6.9	101	18.9	56	7.7	114 (ppm)	276	0.4	3.7	271**	
142807		20.5	47.4	282	30.1	82	30.1	1.58	1.64%	12.9	10.5	1,020	47
142808		1.3	1.2	209	43.9	81	1.3	0.114	451	0.6	8.1	629	78
Roman Ruins chimneys		6	3	190	14.1	1.4	1.7	7.6	23.1%	78	92	2,435	18

CSIRO number	Element:	Br	Rb	Sr	Y	Zr [†]	Mo	Ag	Cd	In	Sb	Te	Cs
	Method:	INAA	ICP-MS	ICP-AES	ICP-MS	ICP-AES	ICP-MS	ICP-AES	ICP-MS	ICP-MS	ICP-MS	ICP-MS	ICP-MS
	Unit: DL:	(ppm) 1	(ppm)	(ppm)	(ppm)	(ppm)	(ppm)	(ppm) 5	(ppm)	(ppm)	(ppm)	(ppm)	(ppb) 10
142701			8.3	10	1.0	15	64	<5	0.58	0.77	2.7	72	71
142703		1	0.3	574	0.9	9	76	<5	1.83	2.8	5.5	0.17	9
142705			0.6	13	0.8	4	76	<5	1.19	0.28	3.5	5.6	60
142807		12	15.0	199	2.3	17	74	15	57	4.2	47	4.9	187
142808		3	1.1	5	0.4	8	46	<5	0.89	0.44	2.0	3.6	64
Roman Ruins chimneys		9	0.8	270	0.05	3	87	250	570	40	550	0.06	260

Table T3 (continued).

CSIRO number	Element:	Ba	La	Ce	Pr	Nd	Sm	Eu	Gd	Tb	Dy	Ho	Er
	Method:	ICP-AES	ICP-MS										
	Unit: DL:	(ppm)	(ppm)	(ppm)	(ppm)	(ppm)	(ppm)	(ppm)	(ppm)	(ppb)	(ppb)	(ppb)	(ppb)
142701		286	4.08	9.28	1.28	5.28	0.97	0.12	0.75	75	254	40	88
142703		78	3.51	8.32	1.27	5.57	1.36	0.78	0.88	95	379	46	89
142705		100	0.56	1.49	0.25	1.32	0.38	0.19	0.38	48	226	35	104
142807		1.04%‡	6.68	14.52	2.03	8.48	1.66	0.71	1.29	155	620	100	235
142808		145	0.74	1.50	0.22	1.04	0.22	0.10	0.19	27	88	22	41
Roman Ruins chimneys		8.8%	1.18	1.32	0.11	0.26	0.04	0.23	0.04	6	14	6	11

CSIRO number	Element:	Tm	Yb	Lu	Hf	W	Au	Hg	Tl	Pb	Bi	Th	U
	Method:	ICP-MS	ICP-MS	ICP-MS	INAA	INAA	INAA	INAA	ICP-MS	ICP-MS	ICP-MS	ICP-MS	ICP-MS
	Unit: DL:	(ppb)	(ppb)	(ppb)	(ppm)	(ppm)	(ppm)	(ppm)	(ppm)	(ppb)	(ppm)	(ppb)	(ppb)
142701		9	87	14					5	78	36	392	687
142703		5	30	7	<1	<2	0.86	5	33	78	15	8	441
142705		9	56	8					116	158	34	11	155
142807		24	148	20	1	11	1.97	6	41	491*	14	159	2,460
142808		9	25	5	<1	<2	1.99	9	27	109	18	31	783
Roman Ruins chimneys		<1	7	1	<1	<2	16.8	7	59	0.24%	1.3	5	950

Notes: CSIRO = Commonwealth Scientific and Industrial Research Organisation, ICP-AES = inductively coupled plasma-atomic emission spectroscopy, ICP-MS = inductively coupled plasma-mass spectrometry, INAA = instrumental neutron activation analysis. Units as noted in column headings except where otherwise noted. DL = detection limit (cited where close to or exceeding some values). Sample 142807 had a white residue present on dissolution; S and Pb may be underestimated. Roman Ruins chimney results are an average of 50 subsamples, from Binns et al. (2000), plus additional data; Si result for Roman Ruins chimneys is an average of 37 subsamples, from Moss and Scott (2001). * = by ICP-AES, † = unreliable data, ‡ = by INAA, unaffected by dissolution problem, ** = by ICP-MS. See Table T1, p. 14, for ODP sample identifications for CSIRO numbers.

Table T4. Isotope data for massive and semimassive sulfides.

CSIRO number	Bulk sulfide					Pyrites
	$^{208}\text{Pb}/^{206}\text{Pb}$	$^{207}\text{Pb}/^{206}\text{Pb}$	$^{206}\text{Pb}/^{204}\text{Pb}$	$^{207}\text{Pb}/^{204}\text{Pb}$	$^{208}\text{Pb}/^{204}\text{Pb}$	^{34}S (‰ CDT)
142701	2.0434	0.82765	18.765	15.531	38.344	1.8, 1.8, 4.0
142703	2.0431	0.82766	18.762	15.529	38.334	2.4, 2.7, 6.3
142705						3.0
142706	2.0427	0.82753	18.761	15.525	38.323	

Notes: CSIRO = Commonwealth Scientific and Industrial Research Organisation, CDT = Canyon Diablo troilite. See Table T1, p. 14, for ODP sample identifications for CSIRO numbers.

Table T5. Normative composition of Leg 193 massive and semimassive sulfides.

CSIRO number	Pyrite	Pyrrhotite*	Chalcopyrite	Sphalerite	Anhydrite	Barite	Silicates
142701	44.7		9.3	0.03	1.3	0.05	44.6
142703	43.7	1.0	14.6	0.10	31.0	0.01	9.6
142705	35.0	4.0	0.0	0.04	0.3	0.02	60.6
142807	60.9	0.6	4.6	2.4	5.3	1.8	24.5
142808	95.0		0.3	0.07	0.1	0.02	4.5

Notes: CSIRO = Commonwealth Scientific and Industrial Research Organisation. See text for calculation method. * = pyrrhotite absent modally, arises from minor analytical errors. See Table T1, p. 14, for ODP sample identifications for CSIRO numbers.

Table T6. Bulk composition of silicates in Leg 193 massive and semimassive sulfides.

CSIRO number	Major element oxides (wt%)									
	SiO ₂	TiO ₂	Al ₂ O ₃	FeO	MnO	MgO	CaO	Na ₂ O	K ₂ O	P ₂ O ₅
142701	90.0	0.37	6.0	0.63	0.01	0.8	0.00	0.4	1.8	0.01
142703	59.5	0.39	15.5		0.46	22.6	0.00	1.5		
142705	99.2	0.01	0.55		0.02	0.02	0.00	0.02	0.07	0.14
142807	57.7	1.33	27.8		0.24	3.3	0.00	2.1	7.4	0.3
142808	57.8	0.40	9.6	22.5	1.15	4.3	0.00	1.8	2.5	

Notes: CSIRO = Commonwealth Scientific and Industrial Research Organisation. Normalized to 100% water-free. FeO = residual Fe after calculation of normative sulfides, CaO = all Ca allocated to anhydrite. See Table T1, p. 14, for ODP sample identifications for CSIRO numbers.